IEEE Access
Multidisciplinary | Rapid Review | Open Access Journal

Received September 5, 2021, accepted September 10, 2021, date of publication September 20, 2021,
date of current version September 29, 2021.

Digital Object Identifier 10.1109/ACCESS.2021.3114260

Model Predictive Control and Adaptive Kalman Filter Design for an Underground Coal Gasification Process

AFRAZ MEHMOOD CHAUDHRY[1], ALI ARSHAD UPPAL[2], (Member, IEEE), AND SVEND BRAM[1]

[1]Department of Engineering Technology, Vrije Universiteit Brussel, 1050 Elsene, Belgium
[2]Department of Electrical and Computer Engineering, COMSATS University Islamabad, Islamabad 45550, Pakistan

Corresponding author: Afraz Mehmood Chaudhry (afraz.mehmood.chaudhry@vub.be)

ABSTRACT The control of a nonlinear system such as an underground coal gasification (UCG) process is a challenging task. Several nonlinear design approaches are implemented to improve the tracking performance of the UCG process, however, the nonlinear techniques make implementation complex and computationally inefficient. In this work, a constrained linear model predictive control (MPC) is designed for the UCG process to track the desired trajectory of the heating value, while satisfying actuator constraints pertaining to UCG. The unknown states required for MPC design are reconstructed by using linear adaptive Kalman filter (AKF) and unscented Kalman filter (UKF). The design of MPC and AKF is based on the quasi-linear model of the UCG process. A fair comparison between different control strategies is conducted which include MPC–AKF, MPC–UKF, MPC–gain scheduled modified Utkin observer (GSMUO) and dynamic integral sliding mode control (DISMC)–GSMUO. The quantitative analysis and simulation results show that MPC-AKF outperforms its counterparts by yielding the least tracking error and average control energy. This conclusion holds, even in the presence of an external disturbance, parametric variations, and measurement and process noises. Moreover, MPC-AKF yields 51%, 44% and 46% improvement in absolute relative root-mean-squared error with reference to MPC–UKF, MPC–GSMUO and DISMC–GSMUO, respectively. A quantitative analysis has also been carried for AKF and UKF, which shows that the performance of AKF is more robust against changes in the initial values of measurement and process covariances.

INDEX TERMS Model predictive control (MPC), underground coal gasification (UCG), adaptive Kalman filter (AKF), unscented Kalman filter (UKF), energy conversion systems.

I. INTRODUCTION

The major share of the world's energy demand is fulfilled by fossil fuels (coal, oil and gas) [1]. Amongst fossil fuels, coal has become the leading energy source for electricity generation [2], [3]. The main reason for its extensive usage is the advent of clean coal technologies such as integrated gasification combined cycle (IGCC) which allows for the extraction of toxic contents at different stages of the process, as discussed in [4]–[6]. In IGCC, coal gasification is integrated with a combined cycle power plant to provide low to medium heating value of syngas (250 to 400 Btu/ft^3), which acts as a fuel for the gas turbine topping cycle. The gasification of coal can be conducted in specially designed chambers known as surface gasifiers or in-situ, also known as underground coal gasification (UCG) [7], [8]. In UCG, the gasification process starts by drilling two wells from the surface to the coal seam. After the link is established between the wells, the already ignited coal seam is gasified by a gas mixture (air and/or steam) injected from the inlet well. The product of UCG is a syngas (a mixture of CO, H_2, CH_4, steam and higher hydrocarbons), which is recovered from the production well [9], [10]. As compared with conventional mining and surface gasification, UCG promises lower capital operating cost and decarbonised product gas [11].

The efficiency of a UCG process can be improved by keeping the heating value of the syngas at the desired level by manipulating the flow rate or molar flux of the inlet gas [12]. This can be achieved by employing an efficient control design of UCG which is an emerging area of research [11].

The associate editor coordinating the review of this manuscript and approving it for publication was Choon Ki Ahn.

Nomenclature

$\bar{e}$	scaled measurement error
δ	input disturbance in terms of flow rate of steam (moles/cm^2/s)
Π, Ξ,Ψ	percentages of H_2O, O_2 and N_2 in u
C_s	specific heat capacity of solids (cal/g/K)
L	length of the reactor (cm)
$q_{i,i}$	diagonal value for process noise covariance matrix
R_i	rate of a chemical reaction (mol/cm^3/s), $i = 1,2,3$ represents pyrolysis, char oxidation and steam gasification, respectively
r_{w}	weighting factor used to bound rate of change of control input
$\alpha_{1,2}$	weighting factor for recursive estimation
$\bar{w}$	scaled state error
β	approximation of spatial derivative (mol/cm^3/s)
Δq_i	heat of reaction i (cal/mol), $i = 1,2$ represents char oxidation and steam gasification, respectively
ρ_i	density of solid i (g/cm^3)
C_i	concentration of gases (mol/cm^3)
h_t	heat transfer coefficient (cal/s/K/cm^3)
M_i	molecular weight (g/mol), $i = 1,2$ for coal and char, respectively
N_{c}	size of control horizon
N_{p}	size of prediction horizon
N_Q	tuning parameter for AKF-R2
N_R	tuning parameter for AKF-R1
P_{g}	gas pressure (atm)
$p_{R_{ij}}$	stoichiometric coefficient $i \in \{1,2,3\}$, $j \in$ {char, CO, CO_2, H_2, CH_4, H_2O, O_2, tar}
T_{s}, T	solid and gas temperatures (K)
u	molar flux of injected gases (mol/cm^2/s)
$v_{i,i}$	diagonal value for sensor noise covariance matrix

A. RELATED WORK

The recent developments and current position of UCG has tended to focus on the control of UCG process [11]. In [13], different control methods pertaining to academic research and experimental research are discussed. Both model-free and model-based control methodologies have been considered for UCG process. In [14] and [15], a conventional Proportional Integral (PI) controller is implemented to regulate the heating value, concentration and temperature of the syngas at the desired levels. The designed controller does not depend on model information explicitly, rather it takes the decision based on available measurements. It is expounded that the measurements of the process variables are considered under the conditions of uncertainties [16]. Therefore, designed control system should be robust enough to handle these uncertainties and continuously adapt the changes taking place in the process [17]. Internet-of-Things (IoT) based wireless sensing system has been introduced for in-situ monitoring and an optimal control is implemented based on deep learning techniques [18]. In [17], an experimental study is demonstrated to show the applicability of optimal control problem with lignite coal based UCG process. The control inputs are generated by solving a real-time optimization problem, which maximize the content of CO in syngas and also ensure the steady state form of syngas. In [19], an experimental and simulation study is conducted by employing an adaptive model predictive control (MPC) for maintaining the calorific value of the syngas at the desired level. The effect of future control inputs on the syngas calorific value to support a predictive control is also analyzed using data-driven design approaches, such as multivariate adaptive regression splines (MARS) [16]. In [20], a model-free optimal control of UCG has been established for continuous optimization of operating variables which results in increased production of syngas. In the aforementioned literature, the designed controllers are either model-free or employ data-driven models. However, the most accurate control and monitoring strategies are model-based, which employ first principle based models of a process [21]. The academic research has produced a set of mathematical models of underground coal gasification, and the European Union-supported program has addressed the production of a decarbonised product gas [11].

In [12], a 1D control-oriented model of the Thar coal UCG process has been proposed. The model has been employed to design a super twisting-based sliding mode control (SMC) and a dynamic SMC for the UCG process in [22] and [23], respectively. The objective of both the controllers is to maintain a desired (constant) heating value of the syngas. Due to the complexity of the model proposed in [12], the controller designs in [22] and [23] bear a lot of assumptions and approximations. The controller design given in [23] is improved by estimating the controller parameters using the artificial neural network (ANN) [24]. Considering the complexity of a partial differential equations (PDEs) based model, a relatively simple model of a UCG process has been proposed in [25], which consists of time-based nonlinear ODEs for mass and energy balances of the UCG process. Moreover, a conventional SMC is also designed for maintaining a desired heating value. In [25], it has been assumed that all the states of the system are measurable, which is not the case practically. This discrepancy has been removed in [26] and [27]. In [26], a gain scheduled modified Utkin observer (GSMUO) along with an integral SMC have been proposed to robustly track the desired trajectory of the heating value. This work has been further improved in [27] with more efficient dynamic integral sliding mode control (DISMC). Apart from the nonlinear techniques discussed above, several model-based linear control techniques have also been designed for the UCG process. In [28], the authors linearized the nonlinear model of [25], using Taylor series approximation around an operating point of interest and designed a linear matrix inequality (LMI) based optimal H_2/H_∞ controller to keep the heating value on a desired level. In [29] and [30], the authors have identified a linear model for the UCG process and then designed H_∞ and dynamic sliding mode controllers based on the identified

linear model, respectively. Furthermore, both the controllers are implemented on the cavity simulation model (CAVSIM) of [31]. As in [28]–[30], the control design is based on linear models, so the controllers are only effective in a limited operating range.

B. GAP ANALYSIS

The nonlinear design frameworks as discussed above make the implementation complex and require more computational resources and cost as discussed in [28]. Due to the ease in the design and implementation of the linear control and estimation techniques, they are extensively used in the process control industry [28]. However, the accuracy of the linear approaches is limited by the degree of nonlinearity and range of the operation of the system. This means that for enjoying the ease of the linear control techniques one has to compromise on the accuracy of the control system. However, in [32] the authors propose a quasi-linear approach which transforms a nonlinear representation of a system into a state space form, comprising of state dependent matrices. Therefore, the quasi-linear approach yields a linear representation of the model, however, the dynamics is still nonlinear. The advantage of such approach is that the linear control and estimation techniques can be designed for nonlinear systems which yield similar performance demonstrated by the conventional nonlinear approaches.

C. MAJOR CONTRIBUTIONS

In this work, the quasi-linear technique of [32] is employed to obtain the exact decomposition of the mass and energy balances of the UCG process. The model is then used to design a model-based constrained linear MPC. The design problem pertaining to the UCG process such as tracking of the desired heating value and minimization of the control input energy is casted in the MPC framework. For the UCG system, the designed MPC successfully solves the optimization problem for robust tracking even in the presence of uncertainties and disturbances. MPC is an effective design approach as it inherently handles the design constraints related to the system. This constraint handling property of MPC is very important and gives it an edge over conventional linear/nonlinear control approaches. As the constraints on states, inputs and outputs are handled inherently, situations like saturation of the actuators can be avoided. In the case of other control techniques, anti-wind-up approaches need to be integrated with the control system to avoid saturation of the actuators. Moreover, the MPC framework includes online optimization at every sampling instant and the current closed-loop input is determined based on the current state of the system. This naturally inculcates robustness in the control framework [33]–[35].

The unknown states of the UCG process, which are required for MPC design are estimated using unscented Kalman filter (UKF) and adaptive Kalman filter (AKF). The designed of linear AKF is also based on the quasi-linear model of UCG. Consequently, a fair comparison has been made between MPC-AKF and its peers, which include combinations of MPC and unscented Kalman filter (MPC-UKF), MPC and gain scheduled modified Utkin observer (MPC-GSMUO), and dynamic integral sliding mode control and GSMUO (DISMC-GSMUO) [27].

The main contribution of this work are as follows:

- A linear MPC, based on the quasi-linear decomposition of the UCG process is designed to track the desired trajectory of the heating value. The designed controller respects the constraints on the input.
- To make the model-based control possible, the unknown states of the system are estimated using AKF and UKF. The design of AKF is also based on a quasi-linear model.
- The designed MPC-AKF methodology is implemented on the nonlinear model of the UCG process. To evaluate the robustness of the designed technique, external disturbance, parametric variations, and process and measurement noises are introduced in the process. A rigorous quantitative comparative analysis is made between the proposed MPC-AKF technique and other linear/nonlinear techniques from the literature, which demonstrates the effectiveness of the designed control scheme.

The rest of the paper is arranged in the following manner. In section II, the nonlinear control-oriented model of the UCG plant is presented. The MPC design is elaborated in section III, whereas, the designs of UKF and AKF are discussed in section IV. The implementation of the proposed methodologies is discussed in section V and this research work is concluded in section VI.

II. MATHEMATICAL MODEL OF UNDERGROUND COAL GASIFICATION PROCESS

In this work, a nonlinear control-oriented model of the UCG process given in [25] is considered. The model is comprised of two solids (coal and char), and eight gases (CO, CO_2, H_2, CH_4, tar, H_2O, O_2 and N_2). The model can be written in nonlinear control-affine form as

$$\dot{\boldsymbol{x}} = \boldsymbol{f}(\boldsymbol{x}) + \boldsymbol{g_1}u + \boldsymbol{g_2}\delta, \tag{1}$$

where $\boldsymbol{x} \in \mathbb{R}^{11\times 1}$ is defined as

$$\boldsymbol{x} = [\rho_{\text{coal}}\ \rho_{\text{char}}\ T_{\text{s}}\ C_{\text{CO}}\ C_{\text{CO}_2}\ C_{\text{H}_2}\ C_{\text{CH}_4}\ C_{\text{tar}}\ C_{\text{H2O}}\ C_{\text{O}_2}\ C_{\text{N}_2}]^{\text{T}}. \tag{2}$$

The vector fields given in Eq. (1) are $\boldsymbol{f}, \boldsymbol{g_1}, \boldsymbol{g_2} \in \mathbb{R}^{11\times 1}$ and given as

$$\boldsymbol{f}(\boldsymbol{x}) = \begin{bmatrix} -M_1R_1 \\ M_2(p_{R_1\text{char}}R_1 - R_2 - R_3) \\ \frac{1}{C_s}\left(h_t(T - T_{\text{s}}) - \Delta q_2\, R_2 - \Delta q_3\, R_3\right) \\ p_{R_1\text{CO}}R_1 + R_3 - \beta C_{\text{CO}} \\ p_{R_1\text{CO}_2}R_1 + R_2 - \beta C_{\text{CO}_2} \\ p_{R_1\text{H}_2}R_1 + R_3 - \beta C_{\text{H}_2} \\ p_{R_1\text{CH}_4}R_1 - \beta C_{\text{CH}_4} \\ p_{R_1\text{tar}}R_1 - \beta C_{\text{tar}} \\ p_{R_1\text{H}_2\text{O}}R_1 + p_{R_2\text{H}_2\text{O}}R_2 - p_{R_3\text{H}_2\text{O}}R_3 - \beta C_{\text{H}_2\text{O}} \\ -p_{R_2\text{O}_2}R_2 - \beta C_{\text{O}_2} \\ -\beta C_{\text{N}_2} \end{bmatrix},$$

$$\boldsymbol{g}_1 = \begin{bmatrix} 0 & 0\,0\,0\,0\,0\,0\,0 & \frac{\Pi}{L} & \frac{\Xi}{L} & \frac{\Psi}{L} \end{bmatrix}^{\mathrm{T}},$$
$$\boldsymbol{g}_2 = \begin{bmatrix} 0 & 0\,0\,0\,0\,0\,0\,0 & \frac{1}{L} & 0 & 0 \end{bmatrix}^{\mathrm{T}}. \quad (3)$$

The control input is represented by u, and δ represents the external disturbance in terms of water influx from the surrounding aquifers [27], [29]. The chemical kinetics is mainly dependent on three chemical reactions which take place in-situ and are stated in Table (1).

TABLE 1. Chemical reactions considered in the UCG. process [27].

No.	Chemical equations
1.	**Coal pyrolysis**
	$\mathrm{CH_{0.912}O_{0.194}} \xrightarrow{R_1} p_{R_1\mathrm{char}}\mathrm{CH_{0.15}O_{0.02}} + p_{R_1\mathrm{CO}}\mathrm{CO} + p_{R_1\mathrm{H_2O}}\mathrm{H_2O} + p_{R_1\mathrm{H_2}}H_2 + p_{R_1\mathrm{CH_4}}\mathrm{CH_4} + p_{R_1\mathrm{CO_2}}\mathrm{CO_2} + p_{R_1\mathrm{tar}}(\mathrm{CH_{2.782}})_9$
2.	**Char oxidation**
	$\mathrm{CH_{0.15}O_{0.02}} + p_{R_2\mathrm{O_2}}\mathrm{O_2} \xrightarrow{R_2} \mathrm{CO_2} + p_{R_2\mathrm{H_2O}}\mathrm{H_2O}$
3.	**Steam gasification**
	$\mathrm{CH_{0.15}O_{0.02}} + p_{R_3\mathrm{H_2O}}\mathrm{H_2O} \xrightarrow{R_3} \mathrm{CO} + \mathrm{H_2}$

The compounds such as $\mathrm{CH_{0.912}O_{0.194}}$, $\mathrm{CH_{0.15}O_{0.02}}$ and $(\mathrm{CH_{2.782}})_9$ represent molecular formulas of coal, char and tar, respectively. The mathematical expressions for the reaction rates of the selected chemical reactions are given as

$$R_1 = 5\frac{\rho_{\mathrm{coal}}}{M_1}\exp\left(\frac{-6039}{T_{\mathrm{s}}}\right), R_{m_2} = \frac{1}{10}h_{\mathrm{t}}m_{\mathrm{O_2}},$$
$$R_{c_2} = \frac{1}{M_2}\left[9.55\times10^{8}\rho_{\mathrm{char}}m_{\mathrm{O_2}}P_{\mathrm{g}}\exp\left(\frac{-22142}{T_{\mathrm{s}}}\right)T_{\mathrm{s}}^{-0.5}\right],$$
$$R_2 = \frac{1}{\frac{1}{R_{c_2}}+\frac{1}{R_{m_2}}}, R_{m_3} = \frac{1}{10}h_{\mathrm{t}}m_{\mathrm{H_2O}},$$
$$R_{c_3} = \frac{\rho_{\mathrm{char}}m_{\mathrm{H_2O}}^2P_{\mathrm{g}}^2\exp\left(5.052-\frac{12908}{T_{\mathrm{s}}}\right)}{M_2\left[m_{\mathrm{H_2O}}P_{\mathrm{g}}+\exp\left(-22.216+\frac{24880}{T_{\mathrm{s}}}\right)\right]^2},$$
$$R_3 = \frac{1}{\frac{1}{R_{c_3}}+\frac{1}{R_{m_3}}}, \quad (4)$$

where $m_{\mathrm{O_2}}$ and $m_{\mathrm{H_2O}}$ are the internal molar fractions of $\mathrm{O_2}$ and $\mathrm{H_2O}$, respectively. Mathematically, the molar fractions are given by

$$m_{\mathrm{O_2}} = \frac{C_{\mathrm{O_2}}}{C_{\mathrm{T}}+C_{\mathrm{H_2O}}}, m_{\mathrm{H_2O}} = \frac{C_{\mathrm{H_2O}}}{C_{\mathrm{T}}+C_{\mathrm{H_2O}}},$$
$$C_{\mathrm{T}} = C_{\mathrm{CO}}+C_{\mathrm{CO_2}}+C_{\mathrm{H_2}}+C_{\mathrm{CH_4}}+C_{\mathrm{tar}}+C_{\mathrm{O_2}}+C_{\mathrm{N_2}}.$$

The stoichiometric coefficients and the nominal parameter values which are used in the nonlinear model of UCG (1) are given in Table (2) and Table (3), respectively.

The product gases are recovered at the production well. After the removal of steam from the gas mixture, the gas analyzer measures the concentration of the following gases

$$\boldsymbol{y_{\mathrm{m}}} = \begin{bmatrix} C_{\mathrm{CO}} & C_{\mathrm{CO_2}} & C_{\mathrm{H_2}} & C_{\mathrm{CH_4}} & C_{\mathrm{tar}} & C_{\mathrm{O_2}} & C_{\mathrm{N_2}} \end{bmatrix}^{\mathrm{T}}. \quad (5)$$

The heating value of the product gases is computed as

$$H_{\mathrm{v}}(x) = H_{\mathrm{CO}}\chi_{\mathrm{CO}} + H_{\mathrm{H_2}}\chi_{\mathrm{H_2}} + H_{\mathrm{CH_4}}\chi_{\mathrm{CH_4}}, \quad (6)$$

where $H_{\mathrm{v}}(x)$ is the heating value of the product gases in kJ/mol. $H_i, i \in \{\mathrm{CO}, \mathrm{H_2}, \mathrm{CH_4}\}$ is the combustion heat (kJ/mol) of gas i and χ_i represents the molar fraction of the gases, given by the ratio

$$\chi_i = \frac{C_i}{C_{\mathrm{T}}}.$$

In order to track the desired trajectory of H_{v}, the design of MPC is presented in the subsequent section.

TABLE 2. Stoichiometric coefficients used in the chemical reactions of the UCG process [27].

$p_{R_1\mathrm{char}}$	$p_{R_1\mathrm{CO}}$	$p_{R_1\mathrm{CO_2}}$	$p_{R_1\mathrm{H_2}}$	$p_{R_1\mathrm{CH_4}}$
0.766	0.008	0.058	0.083	0.044
$p_{R_1\mathrm{tar}}$	$p_{R_1\mathrm{H_2O}}$	$p_{R_2\mathrm{H_2O}}$	$p_{R_3\mathrm{H_2O}}$	$p_{R_2\mathrm{O_2}}$
0.0138	0.055	0.075	0.925	1.02

TABLE 3. Nominal parameter values [27].

C_{s}	β	P	h_{t}	L	Δq_1	Δq_2
[cal/g/K]	[mol/cm^3/s]	[atm]	[cal/s/K/cm^3]	[cm]	[cal/mol]	[cal/mol]
7.3	7×10^{-6}	4.83	0.001	100	-93929	31309

III. MPC DESIGN FOR THE UCG PROCESS

In this section, a constrained linear MPC is designed for the UCG process represented in the control-affine form (1).

A. QUASI-LINEAR DECOMPOSITION OF DISCRETE TIME MODEL OF THE UCG PROCESS

To employ MPC, the nonlinear UCG system in (1) is discretized using the forward Euler method [37], with a step-size of $\Delta t = 2.5$ s to have following nonlinear-discrete form

$$\boldsymbol{x}(k+1) = \boldsymbol{x}(k) + \boldsymbol{f}(\boldsymbol{x}(k)) + \boldsymbol{B}\boldsymbol{u}(k) + \boldsymbol{D}\boldsymbol{\delta}(k),$$
$$\boldsymbol{y}(k) = H_{\mathrm{v}}(\boldsymbol{x}(k)), \quad (7)$$

where $\boldsymbol{f}(\boldsymbol{x}(k)) = \Delta t\boldsymbol{f}(\boldsymbol{x}(t))$, $\boldsymbol{B} = \Delta t\boldsymbol{g}_1$, $\boldsymbol{D} = \Delta t\boldsymbol{g}_2$ and $\boldsymbol{y}(k)$ represent the discrete-time formulation of vectors used in (1), (6). The discrete nonlinear form of UCG (7) is decomposed using a quasi-linear approach given in [32] to yield the following discrete-time state-space representation

$$\boldsymbol{x}(k+1) = \boldsymbol{A}(\boldsymbol{x}(\boldsymbol{k}))\,\boldsymbol{x}(k) + \boldsymbol{B}\boldsymbol{u}(k) + \boldsymbol{D}\boldsymbol{\delta}(k), \quad (8)$$
$$\boldsymbol{y}(k) = \boldsymbol{C}(\boldsymbol{x}(k))\,\boldsymbol{x}(k), \quad (9)$$

where $\boldsymbol{x}(k) \in \mathbb{R}^{11\times1}$, $\boldsymbol{A}(\boldsymbol{x}(k)) \in \mathbb{R}^{11\times11}$, $\boldsymbol{B} \in \mathbb{R}^{11\times1}$ and $\boldsymbol{C}(\boldsymbol{x}(k)) \in \mathbb{R}^{1\times11}$. The matrices $\boldsymbol{A}(\boldsymbol{x}(k))$ and $\boldsymbol{C}(\boldsymbol{x}(k))$

corresponding to the quasi-linear form of $\boldsymbol{f}(\cdot)$ and $H_{\mathrm{v}}(\cdot)$ respectively, are given [27]

$$\begin{aligned}\boldsymbol{A}(\boldsymbol{x}(k)) &= \begin{bmatrix} | & | & & | \\ \boldsymbol{a}_1 & \boldsymbol{a}_2 & \ldots & \boldsymbol{a}_{11} \\ | & | & & | \end{bmatrix}, \\ \boldsymbol{C}(\boldsymbol{x}(k)) &= \begin{bmatrix} \boldsymbol{c}_1 & \boldsymbol{c}_2 & \ldots & \boldsymbol{c}_{11} \end{bmatrix}, \end{aligned} \tag{10}$$

where elements of $\boldsymbol{A}(\boldsymbol{x}(k))$ and $\boldsymbol{C}(\boldsymbol{x}(k))$ are given as

$$\begin{aligned}\boldsymbol{a}_i &= \nabla f_i(\boldsymbol{x}) + \frac{f_i(\boldsymbol{x}) - \boldsymbol{x}^T \nabla f_i(\boldsymbol{x})}{||\boldsymbol{x}||^2}\boldsymbol{x}\ , \quad \boldsymbol{x} \neq \boldsymbol{0}, \\ \boldsymbol{c}_i &= \nabla h_i(\boldsymbol{x}) + \frac{h_i(\boldsymbol{x}) - \boldsymbol{x}^T \nabla h_i(\boldsymbol{x})}{||\boldsymbol{x}||^2}\boldsymbol{x}\ , \quad \boldsymbol{x} \neq \boldsymbol{0}. \end{aligned} \tag{11}$$

The difference of state and control variables is defined as

$$\begin{aligned}\Delta\boldsymbol{x}(k+1) = \boldsymbol{x}(k+1) - \boldsymbol{x}(k); \quad \Delta\boldsymbol{x}(k) = \boldsymbol{x}(k) - \boldsymbol{x}(k-1), \\ \Delta u(k) = u(k) - u(k-1).\end{aligned}$$

The system can be re-written as

$$\Delta\boldsymbol{x}(k+1) = A\Delta\boldsymbol{x}(k) + B\Delta u(k), \tag{12}$$

In the next step, the output $\boldsymbol{y}(k)$ is written in the form of $\Delta\boldsymbol{x}(k)$. A new state variable which combines the $\Delta\boldsymbol{x}(k)$ and $\boldsymbol{y}(k)$ [38], is given as

$$\boldsymbol{x}(k) = [\Delta\boldsymbol{x}(k)\ \boldsymbol{y}(k)]^{\mathrm{T}},$$

Note that

$$\begin{aligned}\boldsymbol{y}(k+1) - \boldsymbol{y}(k) &= C(\boldsymbol{x}(k+1) - \boldsymbol{x}(k)) = C\Delta\boldsymbol{x}(k+1) \\ \boldsymbol{y}(k+1) &= CA\Delta\boldsymbol{x}(k) + CB\Delta u(k),\end{aligned} \tag{13}$$

Equations (12) and (13) lead to the following augmented state-space model

$$\begin{aligned}\overbrace{\begin{bmatrix}\Delta\boldsymbol{x}(k+1) \\ \boldsymbol{y}(k+1)\end{bmatrix}}^{\boldsymbol{x}(k+1)} &= \overbrace{\begin{bmatrix} A & \mathcal{O}^T \\ CA & 1\end{bmatrix}}^{\boldsymbol{A}}\overbrace{\begin{bmatrix}\Delta\boldsymbol{x}(k) \\ \boldsymbol{y}(k)\end{bmatrix}}^{\boldsymbol{x}(k)} + \overbrace{\begin{bmatrix} B \\ CB\end{bmatrix}}^{\boldsymbol{B}}\Delta u(k) \\ \boldsymbol{y}(k) &= \overbrace{\begin{bmatrix}\mathcal{O} & 1\end{bmatrix}}^{\boldsymbol{C}}\begin{bmatrix}\Delta\boldsymbol{x}(k) \\ \boldsymbol{y}(k)\end{bmatrix},\end{aligned} \tag{14}$$

where $\mathcal{O} \in \mathbb{R}^{1\times 11}$ is the vector containing all zeros to formulate augmented form for the UCG system.

B. MPC PROBLEM FORMULATION FOR UCG

The control objective associated with UCG is to track H_{v} to its predefined set-points (r_i) depending upon the operating conditions of the UCG reactor. The control problem also has constraints on the control input $u(k)$ which reflect the characteristics of installed compressors' at the UCG project Thar (UPT). There are two types of constraints associated with the control input. The first constraint comes from the fact that the molar flux cannot be negative and the compressors can only provide a finite value of the maximum molar flux. The second constraint is imposed on the rate of change, $\Delta u(k)$ of the control input. These constraints are given as

$$\begin{aligned}u_{\min} \leq u \leq u_{\max}, \\ \Delta u_{\min} \leq \Delta u \leq \Delta u_{\max},\end{aligned} \tag{15}$$

where $u_{\min} = 0$, $u_{\max} = 5 \times 10^{-4}$, $\Delta u_{\min} = -1.05 \times 10^{-7}$ and $\Delta u_{\max} = 1.05 \times 10^{-7}$. Given an initial state $\boldsymbol{x}(k_i)$ at time index k_i is required to calculate the change in input sequence $\Delta\boldsymbol{U}=\{\Delta u(k_i),\ \Delta u(k_i+1),\ , \ldots., \Delta u(k_i+N_{\mathrm{c}}-1)\}$, where N_{c} is the size of future control trajectories that minimize the cost function of the following form over a finite time horizon N_{p}

$$\mathrm{J} = (\boldsymbol{R_s} - \boldsymbol{Y})^{\mathrm{T}}(\boldsymbol{R_s} - \boldsymbol{Y}) + \Delta\boldsymbol{U}\bar{\boldsymbol{R}}\Delta\boldsymbol{U}, \tag{16}$$

where $\boldsymbol{R_s} = \overbrace{[1\ 1\ \ldots\ 1]}^{N_{\mathrm{p}}\times 1} r(k_i)$ is the column vector that contains the information about the set-points for H_{v}. Here N_{p} denotes the length of the prediction horizon. Furthermore, $r(k_i)$ will remain constant within the defined optimization window N_{p}. $\bar{\boldsymbol{R}}$ is the diagonal matrix of the form $\bar{\boldsymbol{R}} = r_{\mathrm{w}} I_{N_{\mathrm{c}}\times N_{\mathrm{c}}} (r_{\mathrm{w}} > 0)$ and r_{w} is a tuning parameter to bound the rate of change of the control input $\Delta\boldsymbol{U}$. The predicted output $\boldsymbol{Y}$ over a defined horizon N_{p} can be computed as

$$\boldsymbol{Y} = \boldsymbol{F}\boldsymbol{x}(k_i) + \boldsymbol{\phi}\Delta\boldsymbol{U}, \tag{17}$$

where $\boldsymbol{F}$ and $\boldsymbol{\phi}$ are the matrices calculated by using the augmented form given in Eq. (14) over a defined horizons (N_{p} and N_{c}). In this work, the length of both the prediction and control horizon is kept the same, i.e., $N_{\mathrm{p}} = N_{\mathrm{c}}$. The augmented matrices $\boldsymbol{F}$ and $\boldsymbol{\phi}$ are characterized as

$$\begin{aligned}\boldsymbol{F} &= \begin{bmatrix} CA & CA^2 & CA^3 & \ldots & CA^{N_p}\end{bmatrix}^{\mathrm{T}}, \\ \boldsymbol{\phi} &= \begin{bmatrix} CB & 0 & 0 & \ldots & 0 \\ CAB & CB & 0 & \ldots & 0 \\ CA^2B & CAB & CB & \ldots & 0 \\ . & & & & \\ . & & & & \\ . & & & & \\ CA^{N_{\mathrm{p}}-1}B & CA^{N_{\mathrm{p}}-2}B & CA^{N_{\mathrm{p}}-3}B & \ldots & CA^{N_{\mathrm{p}}-N_{\mathrm{c}}}B \end{bmatrix}.\end{aligned} \tag{18}$$

Now, by substituting $\boldsymbol{Y}$ in (16), the cost function can be re-written as

$$\begin{aligned}\mathrm{J} = (\boldsymbol{R_s} - (\boldsymbol{F}\boldsymbol{x}(k_i) + \boldsymbol{\phi}\Delta\boldsymbol{U}))^T(\boldsymbol{R_s} - (\boldsymbol{F}\boldsymbol{x}(k_i) \\ + \boldsymbol{\phi}\Delta\boldsymbol{U})) + \Delta\boldsymbol{U}\bar{\boldsymbol{R}}\Delta\boldsymbol{U}.\end{aligned} \tag{19}$$

Moreover, $\Delta\boldsymbol{U}$ in the given cost function (19) also has the process design constraints pertaining to the UCG process, which are of the form (15) as discussed earlier. Thus, the optimization problem of the MPC can be transformed as to find the optimal control parameter vector ($\Delta\boldsymbol{U}$) that satisfies the constraints of the form (15) while minimizing the cost function given in (16).

These constraints can be re-written as

$$\Delta\,\boldsymbol{U}_{\min} \leq \Delta\boldsymbol{U}(k_i) \leq \Delta\,\boldsymbol{U}_{\max}, \tag{20}$$

and in a matrix form as

$$\begin{bmatrix} -I \\ +I \end{bmatrix} \Delta U \leq \begin{bmatrix} -\Delta\, \boldsymbol{U}_{\min} \\ +\Delta\, \boldsymbol{U}_{\max} \end{bmatrix}. \tag{21}$$

In case of constraint on amplitude $[u_{\min}, u_{\max}]$, control variable $u(k_i)$ is manipulated in terms of a parameterized variable as

$$\begin{bmatrix} u(k_i) \\ u(k_i+1) \\ u(k_i+2) \\ . \\ . \\ . \\ u(k_i+N_c-1) \end{bmatrix} = \begin{bmatrix} 1 \\ 1 \\ 1 \\ . \\ . \\ . \\ 1 \end{bmatrix} u(k_i-1) + \begin{bmatrix} 1\,0\,0\ldots 0 \\ 1\,1\,0\ldots 0 \\ 1\,1\,1\ldots 0 \\ . \\ . \\ . \\ 1\,1\,1\,.\,.\,1\,1 \end{bmatrix} \begin{bmatrix} \Delta u(k_i) \\ \Delta u(k_i+1) \\ \Delta u(k_i+2) \\ . \\ . \\ . \\ \Delta u(k_i+N_c-1) \end{bmatrix}.$$

Let C_1 and C_2 be the matrices of an appropriate dimension and with the manipulated variable $u(k_i) = u(k_i-1)+\Delta \boldsymbol{U}(k_i)$ yields the following form of the inequality in (20)

$$-\boldsymbol{U}_{\min} \leq (C_1\, u(k_i-1) + C_2 \Delta \boldsymbol{U}) \leq \boldsymbol{U}_{\max}, \tag{22}$$

where $\boldsymbol{U}_{\min}$ and $\boldsymbol{U}_{\max} \in R^{N_c \times 1}$ are column vectors of $u_{\min}$ and $u_{\max}$, respectively. Similarly, in case of control variation or rate of change of the control input, the constraints given in (21) can be considered. Where $\Delta \boldsymbol{U}_{\min}$ and $\Delta \boldsymbol{U}_{\max}$ are column vectors with N_c elements of $\Delta u_{\min}$ and $\Delta u_{\max}$, respectively. Furthermore, both constraints are coupled in the following form

$$\begin{bmatrix} M_1 \\ M_2 \end{bmatrix} \Delta U \leq \begin{bmatrix} N_1 \\ N_2 \end{bmatrix}, \tag{23}$$

where the matrices M_1, M_2, N_1 and N_2 are given as

$$M_1 = \begin{bmatrix} -C_1 \\ +C_2 \end{bmatrix}, \quad N_1 = \begin{bmatrix} -\boldsymbol{U}_{\min} + C_1\, u(k_i-1) \\ +\boldsymbol{U}_{\max} + C_1\, u(k_i-1) \end{bmatrix},$$
$$M_2 = \begin{bmatrix} -I \\ +I \end{bmatrix}, \quad N_2 = \begin{bmatrix} -\Delta \boldsymbol{U}_{\min} \\ +\Delta \boldsymbol{U}_{\max} \end{bmatrix}. \tag{24}$$

In order to estimate the unknown states required for the MPC design, two types of KFs are discussed in the following section.

IV. KALMAN FILTER-BASED STATE ESTIMATION OF THE UCG PROCESS

As discussed in section II, 7 out of 11 states of the UCG process are measured using the gas analyzer. These states are given in the measurement vector $\boldsymbol{y_m}$ (5). The remaining four states, which include ρ_{coal}, ρ_{char}, T_s and C_{H_2O} are not measurable. Therefore, in order to estimate these unknown states, we designed KF-based estimators. It is pertinent to mention that for the UCG system, the exact noise covariances are not known. Whereas, uncertain and biased values of initial covariances may result in divergence or degradation of the estimator [39], [40]. Thus, the designed estimator should be robust enough to handle the true values of these covariances which may arise at the commissioning stage of the plant. In view of this, two different KF-based estimators are designed, one from a nonlinear design approach known as UKF and another from on extended linear KF-based approach known as AKF [41]. For both designs, the discrete-time nonlinear system of UCG (7) as discussed in section III-A is considered and given as

$$\begin{aligned} \boldsymbol{x_{k+1}} &= \boldsymbol{f}(\boldsymbol{x_k}, \boldsymbol{u_k}) + \boldsymbol{B}(\boldsymbol{u_k}) + \boldsymbol{D}(\boldsymbol{\delta_k}) + \boldsymbol{w_k}, \\ \boldsymbol{y_{m_k}} &= \mathrm{H}\boldsymbol{x_k} + \boldsymbol{v_k}, \\ \mathrm{H} &= \begin{bmatrix} 0\,0\,0\,1\,0\,0\,0\,0\,0\,0\,0 \\ 0\,0\,0\,0\,1\,0\,0\,0\,0\,0\,0 \\ 0\,0\,0\,0\,0\,1\,0\,0\,0\,0\,0 \\ 0\,0\,0\,0\,0\,0\,1\,0\,0\,0\,0 \\ 0\,0\,0\,0\,0\,0\,0\,1\,0\,0\,0 \\ 0\,0\,0\,0\,0\,0\,0\,0\,0\,1\,0 \\ 0\,0\,0\,0\,0\,0\,0\,0\,0\,0\,1 \end{bmatrix}, \\ \boldsymbol{w_k} &\sim \mathcal{N}(0, \boldsymbol{Q_k}), \\ \boldsymbol{v_k} &\sim \mathcal{N}(0, \boldsymbol{R_k}), \\ E[(\boldsymbol{v_k}\boldsymbol{v_j}^T)] &= R_k \delta_{k-j}, \\ E[(\boldsymbol{w_k}\boldsymbol{w_j}^T)] &= Q_k \delta_{k-j}, \\ E[(\boldsymbol{w_k}\boldsymbol{v_j}^T)] &= 0, \end{aligned} \tag{25}$$

where the kronecker delta function $\delta_{k-j} = 1$ if $k = j$ and $\delta_{k-j} = 0$ if $k \neq j$. $\boldsymbol{w_k}$ and $\boldsymbol{v_k}$ represent process and measurement noises. Both noises are white, zero mean, uncorrelated and with known covariance matrices $\boldsymbol{Q}_k \in \mathbb{R}^{11\times 11}$ and $\boldsymbol{R}_k \in \mathbb{R}^{7\times 7}$, respectively.

A. UNSCENTED KALMAN FILTER DESIGN

The UKF is implemented for UCG states reconstruction in three steps which are usually followed in any KF-based design [40]

Step I: Initialization

The initial values of posteriori state estimate ($\hat{\boldsymbol{x}}_0^+$), posteriori state estimation error covariance matrix ($\boldsymbol{P}_0^+$), and process ($\boldsymbol{Q}_0$) and measurement ($\boldsymbol{R}_0$) noise covariance matrices are given as

$$\begin{aligned} \hat{\boldsymbol{x}}_0^+ &= E(\hat{\boldsymbol{x}}_0)\,, \\ \boldsymbol{P}_0^+ &= E[(\boldsymbol{x}_0 - \hat{\boldsymbol{x}}_0^+)(\boldsymbol{x}_0 - \hat{\boldsymbol{x}}_0^+)^{\mathrm{T}}], \\ \boldsymbol{Q}_0 &= \mathrm{diag}\,\left(q_{1,1},\, q_{2,2},\, \cdots q_{11,11}\right), \\ \boldsymbol{R}_0 &= \mathrm{diag}\,\left(v_{1,1},\, v_{2,2},\, \cdots v_{7,7}\right), \end{aligned} \tag{26}$$

where $q_{i,i}$ and $v_{i,i}$ are the diagonal values of covariance matrices $\boldsymbol{Q}_0$ and $\boldsymbol{R}_0$ respectively.

Step II: Time Update

After initialization, the next step is to propagate the state estimates and covariance to the next time step. To achieve this the sigma points are computed as

$$\boldsymbol{x}^{(i)} = \bar{\boldsymbol{x}} + \tilde{\boldsymbol{x}}^{(i)}, \quad i = 1, \ldots, 2n$$

$$\tilde{\boldsymbol{x}}^{(i)} = (\sqrt{n\boldsymbol{P}})_i^{\mathrm{T}}, \quad i = 1, \ldots, n$$
$$\tilde{\boldsymbol{x}}^{(n+i)} = -(\sqrt{n\boldsymbol{P}})_i^{\mathrm{T}}. \quad i = 1, \ldots, n, \tag{27}$$

For the time update step of UKF, the mean and covariance of a vector $\boldsymbol{x}$ will be transformed through sigma points given in Eq. (27) as

$$\boldsymbol{x}^{(i)} = \boldsymbol{x}_{k-1}^{(+)} + \tilde{\boldsymbol{x}}^{(i)}, \quad i = 1, \ldots, 2n$$
$$\tilde{\boldsymbol{x}}^{(i)} = \left(\sqrt{n\boldsymbol{P}_{k-1}^{(+)}}\right)_i^{\mathrm{T}}, \quad i = 1, \ldots, n$$
$$\tilde{\boldsymbol{x}}^{(n+i)} = -\left(\sqrt{n\boldsymbol{P}_{k-1}^{(+)}}\right)_i^{\mathrm{T}}. \quad i = 1, \ldots, n, \tag{28}$$

by using the known nonlinear form of UCG $\boldsymbol{f}(\cdot)$, the sigma points will be transformed as

$$\hat{\boldsymbol{x}}_k^{(i)} = f(\hat{\boldsymbol{x}}_{k-1}^{(i)}, \boldsymbol{u}_k), \tag{29}$$

$\hat{\boldsymbol{x}}_k^{(i)}$ can be combined with the following form

$$\hat{\boldsymbol{x}}_k^{-} = W \sum_{i=1}^{2n} \hat{\boldsymbol{x}}_k^{(i)}, \tag{30}$$

where $W = \frac{1}{2n}$ for $i = 1, 2, \ldots, 2n$ is the weight coefficient to match the priori estimate ($\hat{\boldsymbol{x}}_k^{-}$) as given in (29) with transformed sigma points at time k. Similarly, the priori estimate of state estimation error covariance matrix ($\boldsymbol{P}_k^{-}$) can also be computed as

$$\boldsymbol{P}_k^{-} = W \sum_{i=1}^{2n} (\hat{\boldsymbol{x}}_k^{(i)} - \hat{\boldsymbol{x}}_k^{-})(\hat{\boldsymbol{x}}_k^{(i)} - \hat{\boldsymbol{x}}_k^{-})^{\mathrm{T}}. \tag{31}$$

Step III: Measurement Update

In measurement update, H given in Eq. (25) is used to transform the sigma points $\boldsymbol{y}_k^{(i)}$ into $\hat{\boldsymbol{y}}_k^{(i)}$ as

$$\hat{\boldsymbol{y}}_k^{(i)} = \mathrm{H}\hat{\boldsymbol{x}}_k^{(i)}, \tag{32}$$

where $\hat{\boldsymbol{x}}_k^{(i)}$ are based on same sigma points as given in Eq. (29). By combining $\hat{\boldsymbol{y}}_k^{(i)}$ vector yields the predicted measurement at current time k

$$\hat{\boldsymbol{y}}_k = W \sum_{i=1}^{2n} \hat{\boldsymbol{y}}_k^{(i)}. \tag{33}$$

In the same way, the measurement covariance error matrix ($\boldsymbol{P}_y$) can be calculated as

$$\boldsymbol{P}_y = W \sum_{i=1}^{2n} (\hat{\boldsymbol{y}}_k^{(i)} - \hat{\boldsymbol{y}}_k)(\hat{\boldsymbol{y}}_k^{(i)} - \hat{\boldsymbol{y}}_k)^{\mathrm{T}} + \boldsymbol{R}_k. \tag{34}$$

$\boldsymbol{R}_k$ is added to take the measurement noise into account. For UKF-based design cross covariance between $\hat{\boldsymbol{x}}_k^{-}$ and $\hat{\boldsymbol{y}}_k$ is calculated as [40]

$$\boldsymbol{P}_{xy} = W \sum_{i=1}^{2n} (\hat{\boldsymbol{x}}_k^{(i)} - \hat{\boldsymbol{x}}_k^{-})(\hat{\boldsymbol{y}}_k^{(i)} - \hat{\boldsymbol{y}}_k)^{\mathrm{T}}. \tag{35}$$

In the end, the measurement update is performed

$$\boldsymbol{K}_k = \boldsymbol{P}_{xy}\boldsymbol{P}_y^{-1}, \tag{36}$$
$$\hat{\boldsymbol{x}}_k^{+} = \hat{\boldsymbol{x}}_k^{-} + \boldsymbol{K}_k(\boldsymbol{y}_k - \hat{\boldsymbol{y}}_k), \tag{37}$$
$$\boldsymbol{P}_k^{+} = \boldsymbol{P}_k^{-} - \boldsymbol{K}_k\boldsymbol{P}_y\boldsymbol{K}_k^{\mathrm{T}}. \tag{38}$$

The results of UKF are discussed in section V. In the proposed UKF algorithm, the process and measurement noise covariances are not adapted. This motivates to design AKF to adapt initial unknown biased values of process and measurement noise covariances.

B. ADAPTIVE KALMAN FILTER DESIGN

The main advantage of AKF is the adaptation of unknown biased initial process and measurement covariances in the environment where the true values of these covariances are not known [39], [42]. As discussed earlier, the true values of process and measurement noise covariances are unknown. The initial values of process noise covariance matrix $\boldsymbol{Q}_0$ and measurement noise covariance matrix $\boldsymbol{R}_0$ affect $\hat{\boldsymbol{x}}_k$. If $\boldsymbol{Q}_0$ and $\boldsymbol{R}_0$ are too small then $\hat{\boldsymbol{x}}_k$ may be biased with some estimation error and if $\boldsymbol{Q}_0$ and $\boldsymbol{R}_0$ are too large then $\hat{\boldsymbol{x}}_k$ can oscillate [39]. However, in order to counter the initial unknown biased covariances ($\boldsymbol{Q}_0$ and $\boldsymbol{R}_0$), the AKF design approach is implemented for the UCG system.

The working principle of AKF is based on the extended KF [41], which employs a linear representation of the system for estimation [42], [40]. However, any mismatch between the actual model and the linear model may cause poor performance of the designed KF [42] and [40]. For the UCG system, the quasi-linear approach provides the exact decomposition which is required by the AKF algorithm. The algorithm of AKF is discussed in the next paragraphs.

The initial step for AKF is similar to UKF which is given in Eq. (26). The rules **R1** and **R2** are implemented by modifying the time update and the measurement update steps of the conventional KF, [39].

R1: Measurement covariance update rule

The adaptation of $\boldsymbol{R}_k$ is calculated with the measurement error update in Eq. (41), which uses the conventional time update step of KF equations given in Eqs. (39) and (40), respectively.

$$\hat{\boldsymbol{x}}_k^{-} = \boldsymbol{A}(\boldsymbol{x}(\boldsymbol{k}))\hat{\boldsymbol{x}}_{k-1} + \boldsymbol{B}\boldsymbol{u}_{k-1}, \tag{39}$$
$$\boldsymbol{P}_k^{-} = \boldsymbol{A}(\boldsymbol{x}(\boldsymbol{k}))\boldsymbol{P}_{k-1}(\boldsymbol{A}(\boldsymbol{x}(\boldsymbol{k})))^{\mathrm{T}} + \boldsymbol{Q}_{k-1}, \tag{40}$$
$$\boldsymbol{e}_k = \boldsymbol{z}_k - \mathrm{H}\hat{\boldsymbol{x}}_k^{-}, \tag{41}$$
$$\alpha_1 = \frac{N_R - 1}{N_R}, \tag{42}$$
$$\bar{\boldsymbol{e}}_k = \alpha_1\bar{\boldsymbol{e}}_{k-1} + \frac{1}{N_R}\boldsymbol{e}_k, \tag{43}$$
$$\Delta\boldsymbol{R}_k = \frac{1}{N_R - 1}(\boldsymbol{e}_k - \bar{\boldsymbol{e}}_k)(\boldsymbol{e}_k - \bar{\boldsymbol{e}}_k)^{\mathrm{T}} - \frac{1}{N_R}\mathrm{H}\boldsymbol{P}_k^{-}\mathrm{H}^{\mathrm{T}}, \tag{44}$$
$$\boldsymbol{R}_k = \mid \mathrm{diag}(\alpha_1\boldsymbol{R}_{k-1} + \Delta\boldsymbol{R}_k) \mid . \tag{45}$$

R2: Process covariance update rule

Similarly, for the adaptation of $\boldsymbol{Q}_k$, we need to calculate the state estimation error in Eq. (49) by using the conventional KF design step of measurement update Eqs. (46) to (48).

$$\boldsymbol{K}_k = \boldsymbol{P}_k^- \mathrm{H}^\mathrm{T}(\mathrm{H}\boldsymbol{P}_k^- \mathrm{H}^\mathrm{T} + \boldsymbol{R}_k)^{-1}, \tag{46}$$

$$\hat{\boldsymbol{x}}_k = \hat{\boldsymbol{x}}_k^- + \boldsymbol{K}_k \boldsymbol{e}_k, \tag{47}$$

$$\boldsymbol{P}_k = (\boldsymbol{I} - \boldsymbol{K}_k \mathrm{H})\boldsymbol{P}_k^-, \tag{48}$$

$$\hat{\boldsymbol{w}}_k = \hat{\boldsymbol{x}}_k - \hat{\boldsymbol{x}}_k^-, \tag{49}$$

$$\alpha_2 = \frac{N_Q - 1}{N_Q}, \tag{50}$$

$$\bar{\boldsymbol{w}}_k = \alpha_2 \bar{\boldsymbol{w}}_{k-1} + \frac{1}{N_Q}\hat{\boldsymbol{w}}_k, \tag{51}$$

$$\Delta\boldsymbol{Q}_k = \frac{1}{N_Q}(\boldsymbol{P}_k - \boldsymbol{A}(\boldsymbol{x}(k))\boldsymbol{P}_k^-(\boldsymbol{A}(\boldsymbol{x}(k)))^\mathrm{T}) + \frac{1}{N_Q - 1}(\hat{\boldsymbol{w}}_k - \bar{\boldsymbol{w}}_k)(\hat{\boldsymbol{w}}_k - \bar{\boldsymbol{w}}_k)^\mathrm{T}, \tag{52}$$

$$\boldsymbol{Q}_k = |\ \mathrm{diag}(\alpha_2 \boldsymbol{Q}_{k-1} + \Delta\boldsymbol{Q}_k)\ |\ . \tag{53}$$

The implementation of AKF is shown in Fig. (1). The performance of both AKF and UKF against different biased covariances is analyzed in the following section.

V. SIMULATION RESULTS AND DISCUSSIONS

In order to evaluate the robust performance of the designed AKF and UKF with the proposed MPC scheme, the simulations are conducted by using a closed-loop configuration of UCG as shown in Fig. (2). Moreover, the performance of AKF and UKF is also compared with GSMUO designed in [27].

The formulated optimization problem of MPC in Eq. (16) is solved for UCG while satisfying the constraints given in Eq. (15) using the `fmincon` function in MATLAB. In `fmincon`, the sequential quadratic programing (`sqp`) algorithm is used. The system specifications to run the simulations are: (i) processor 2.6 GHz, 6-Core Intel Core i7 and (ii) memory 16 GB. The options selected for `fmincon` are: (i) maximum iterations = 30, (ii) functional tolerance = 10^{-6}, (iii) constraint tolerance= 10^{-6} and (iv) step-size tolerance = 10^{-6}. The resultant operating sequence $\{\Delta u(0)^*,\ \Delta u(1)^*, \ldots, \Delta u(k_i + N_\mathrm{c} - 1)^*\}$ is calculated for the defined prediction horizon (N_p= 5). The initial conditions and parameters are given in Table (4). From Fig. (2), it can be observed that MPC needs full state information of the system which is provided by UKF, AKF and GSMUO. As discussed earlier, true values of noise covariances are unknown. Therefore, the designed estimators are tested against uncertain initial covariances in the closed-loop configuration in Fig. (2).

The performance of MPC is evaluated against parametric variations, disturbance in terms of water influx flow rate (δ) and sensor noise. In order to represent the plant-model mismatch, the process noise $\boldsymbol{w}$ is also considered. Additionally, as discussed in section III-B, actuator constraints which reflect the installed compressor limitations are also incorporated in the design. Parametric uncertainties of 2%, as given in Table (5) are also included in the nominal model parameters of the UCG plant namely, P, β, h_t and C_s to validate the robustness property of the designed control and estimation strategies.

TABLE 4. Description of parameters.

Symbol	Value
$\boldsymbol{x_0}$	$[0.5\ 0\ 497\ 0\ 0\ 0\ 0\ 0\ 0\ 4.2e{-}4\ 1.6e{-}3]^\mathrm{T}$
$\hat{\boldsymbol{x}}_0^+$	$[0.48\ 0\ 480\ 0\ 0\ 0\ 0\ 0\ 0\ 4.2e{-}4\ 1.6e{-}3]^\mathrm{T}$
$q_{i,i}$	10^{-7}
$\boldsymbol{w}$	10^{-4}
$\boldsymbol{\nu}$	4×10^{-4}
$\boldsymbol{Q}_0$	$q_{i,i} \times \mathrm{I}_{11}$
$v_{i,i}$	4×10^{-4}
$\boldsymbol{R}_0$	$v_{i,i} \times \mathrm{I}_7$
N_R	$7{\times}10^5$
N_Q	$5{\times}10^5$
$\bar{e}_0$	$[1\ 1\ 1\ 1\ 1\ 1\ 1\ ]^\mathrm{T}$
$\bar{w}_0$	$10^{-4} \times [1\ 1\ 1\ 1\ 1\ 1\ 1\ 1\ 1\ 1\ 1]^\mathrm{T}$
N_p	5
N_c	5
r_w	1.2

TABLE 5. Parameters subjected to perturbations.

Symbol	Nominal Value	Actual Value
C_s	7.3920	7.2440
β	7×10^{-6}	6.86×10^{-6}
P	4.83	4.93
h_t	0.0010	0.00102

It is worth mentioning that both the MPC and the estimators use the nominal system parameters. The disturbance profile which represents the flow rate δ of steam due to water influx from the surrounding aquifers is given in Fig. (3), and it acts as an input disturbance.

In the simulations, the UCG system operates in open-loop for $t < 5.5$ hr. During this time the molar flux of injected gas mixture is fixed at $u = 2 \times 10^{-4}$ mol/cm^2/s. This strategy is adopted so that the H_v reaches the vicinity of its desired set-point [25], [27]. At $t = 5.5$ hr, the MPC starts its operation and tracks the reference trajectory of H_v as shown in Fig. (4). It is pertinent to mention here that the estimators operate for the full length of the simulation. The open-loop operation of the estimators allows to overcome the initial state estimation errors. The tracking errors for different state estimators have been shown in Fig. (5). Similarly, the control effort with different estimators is demonstrated in Fig. (6). It can be seen in Fig. (6) that with the increase in δ, the controller increases the injection of more oxidants which maintains the desired temperature of the UCG reactor and ultimately the desired concentrations of product gases as shown in Figs. (8–13). Furthermore, the root-mean-squared (RMS) values of the tracking error (e_rms) and average power of the control signal (p_avg) are given as

$$e_\mathrm{rms} = \sqrt{\frac{1}{N}\sum_{i=1}^{N} e(i)^2},\ e(i) = H_\mathrm{v}(i) - R_\mathrm{s}(i), \tag{54}$$

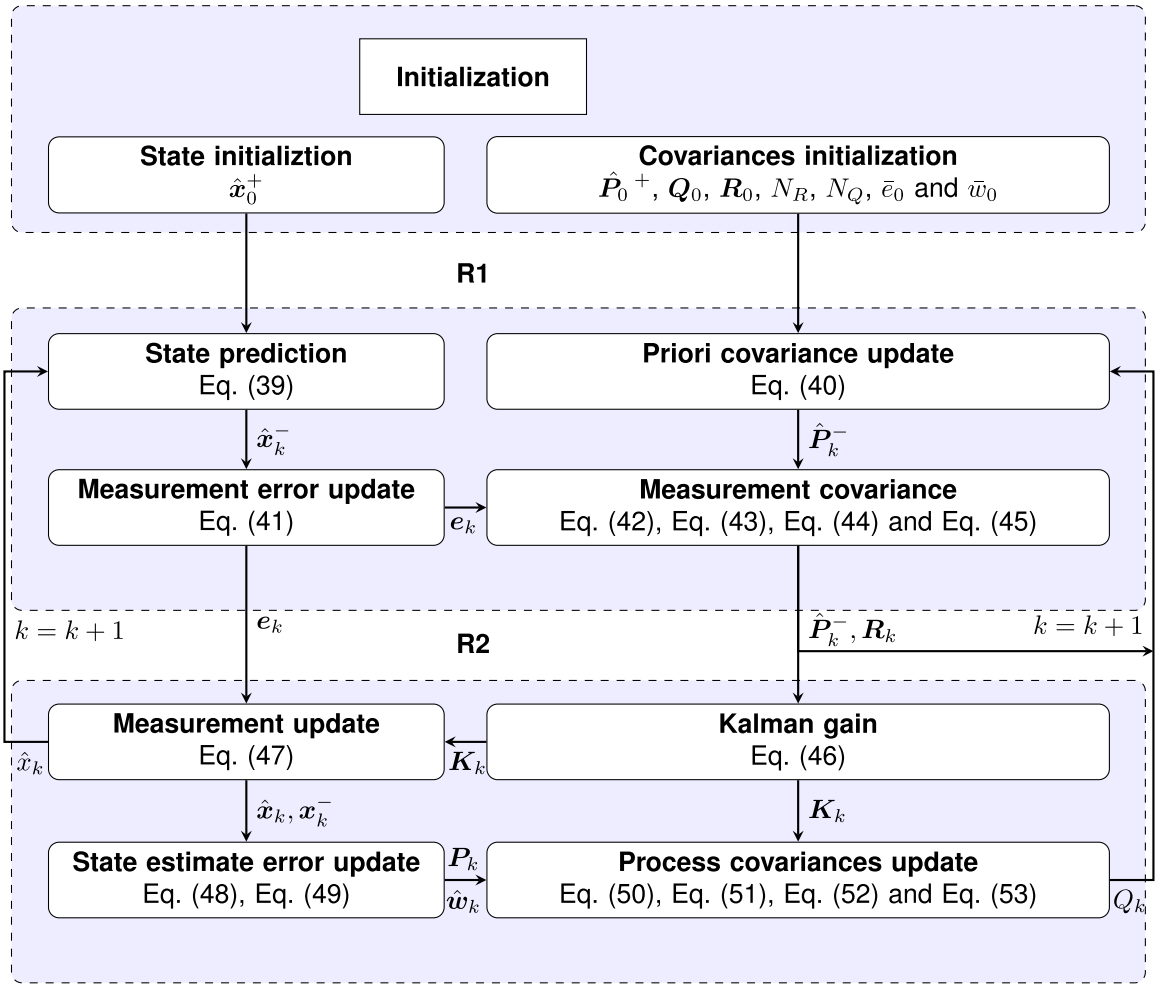

FIGURE 1. AKF implementation for the robust estimation of the UCG system.

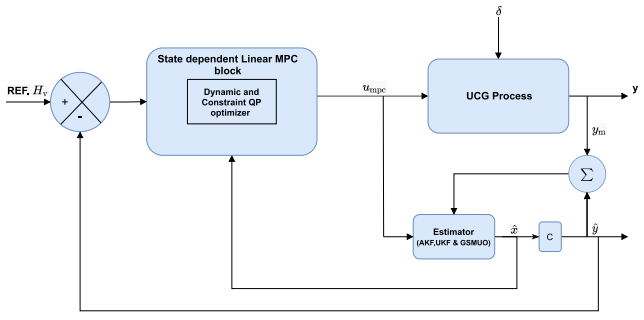

FIGURE 2. Overview of the overall control implementation scheme for the UCG process.

$$p_{\text{avg}} = \frac{1}{N}\sum_{i=1}^{N} u(i)^2, \tag{55}$$

where $R_s(i)$ represents the desired set-point of H_v. The results in Table (6) show that MPC-AKF outperforms MPC-GSMUO, MPC-UKF and DISMC-GSMUO [27] by consuming the least control energy while yielding the minimum e_{rms}.

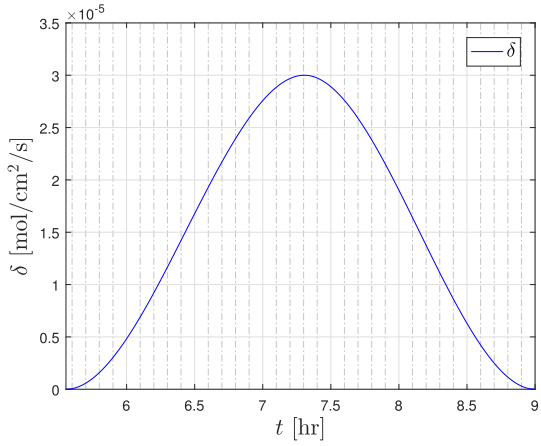

FIGURE 3. Flow rate of water influx from surrounding aquifers.

Moreover, the absolute relative tracking error improvement for MPC–AKF (E[MPC-AKF]) with reference to other control techniques is computed as

$$\text{E[MPC-AKF]} = \frac{e_{\text{rms}[\varkappa]} - e_{\text{rms[MPC-AKF]}}}{e_{\text{rms}[\varkappa]}} \ [\%], \tag{56}$$

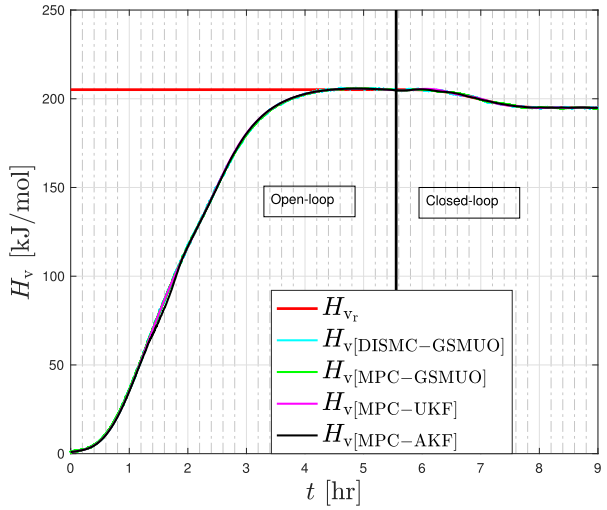

FIGURE 4. Evolution of the heating value of the UCG process.

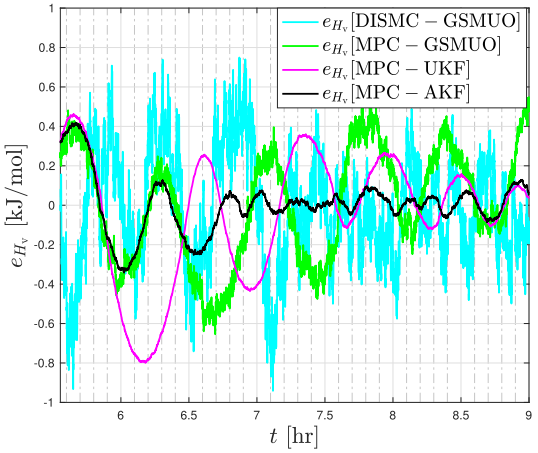

FIGURE 5. Tracking error for different control schemes.

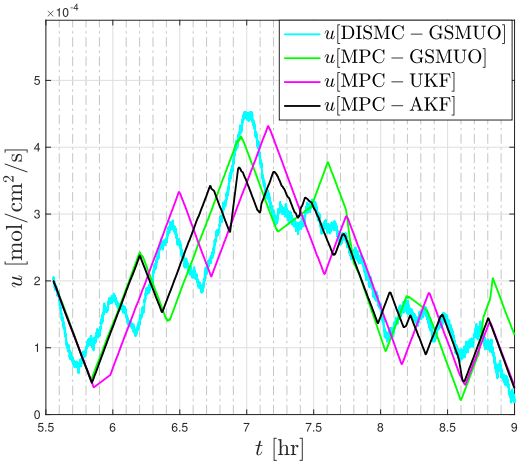

FIGURE 6. Control input (molar flux of injected gases) for different control schemes.

where $e_{\text{rms}[x]}$ is the tracking error of MPC–UKF, MPC–UKF and DISMC–GSMUO. By using the results of Table (6) in Eq. (56), it can be seen that MPC-AKF yields 51%, 44% and 46% improvement in absolute relative root-mean-squared error with reference to MPC–UKF, MPC–GSMUO and DISMC–GSMUO, respectively.

TABLE 6. The e_{rms} and p_{avg} for different control schemes.

Controller with Estimator	e_{rms}[kJ/mol]	p_{avg}[mol/cm^2/s]
DISMC with GSMUO [27]	0.288	5.069×10^{-8}
MPC with GSMUO	0.280	5.256×10^{-8}
MPC with UKF	0.318	5.050×10^{-8}
MPC with AKF	0.156	4.875×10^{-8}

Both UKF and AKF filters discussed in section IV are initialized using parameters given in Table (4). For small values of N_R and N_Q, AKF performs poorly in terms of estimation error. Thus, for UCG the large values of N_R and N_Q are selected as they give more weight to the recursive values ($\boldsymbol{R}_{k-1}$,$\boldsymbol{Q}_{k-1}$) as compared to the current noisy values of $\Delta\boldsymbol{R_k}$ and $\Delta\boldsymbol{Q_k}$ in adaptation of $\boldsymbol{R_k}$ and $\boldsymbol{Q_k}$ as given in Eq. (45) and Eq. (53), respectively. Moreover, the AKF gain is changed based on the adaptation of $\boldsymbol{R_k}$ and $\boldsymbol{Q_k}$ through measurement error update (e_k) in Eq. (41) and state estimation error update ($\hat{w}_k$) in Eq. (49) respectively. Thus, if the tracking is not satisfied then the gain will not converge to a small value. The performance of AKF and UKF estimators is evaluated in terms of the root-mean-squared error defined as

$$\tilde{e}_{\text{rms}} = \sqrt{\frac{1}{N}\sum_{i=1}^{N}\tilde{e}(i)^2}, \;\; \tilde{e}(i) = x(i) - \hat{x}(i), \tag{57}$$

The $\tilde{e}_{\text{rms}}$ is calculated for different initial biased values of $\boldsymbol{Q}_0$ and $\boldsymbol{R}_0$ in Table (7). The initial values are changed using Eq. (26) by selecting different values of $q_{i,i}$ and $v_{i,i}$ for Cases: 1, 2 and 3, respectively. It is pertinent to mention that the process noise variance $w = 10^{-4}$ and sensor noise variance $v = 4 \times 10^{-4}$ for the UCG plant remain the same for all cases listed below:

- **Case 1 ($q_{i,i} = 10^{-7}$ and $v_{i,i} = 4 \times 10^{-4}$):** In Fig. (7-a), the standard deviation (σ) of $\boldsymbol{q}_{2,2}$ is shown to represent the adaptation for ρ_{char}. The initial small values of $\boldsymbol{R_0}$ and $\boldsymbol{Q_0}$ are adapted according to Eq. (45) and Eq. (53), respectively. Consequently, the Kalman gain in Eq. (46) converges to a smaller value. Thus, the $\tilde{e}_{\text{rms}}$ values of AKF are close to UKF as calculated in Table (7).
- **Case 2 ($q_{i,i} = 10^{-5}$ and $v_{i,i} = 2 \times 10^{-2}$):** In Fig. (7-b), the adaption is shown for the Case 2. The relatively larger values of $\boldsymbol{R_0}$ and $\boldsymbol{Q_0}$ result in increased Kalman gain which improves the performance of AKF as compared to UKF as calculated in Table (7).
- **Case 3 ($q_{i,i} = 10^{-4}$ and $v_{i,i} = 2 \times 10^{-2}$):** As compared to Case 2, the value of $q_{i,i}$ is further increased. It can be observed in Table 7 that the performance of AKF is slightly improved due to slight increase in Kalman gain, however, the performance of UKF is deteriorated due to increase in $q_{i,i}$.

The performance of AKF, UKF and GSMUO has been shown in Figs. (8–13). It is pertinent to mention here that

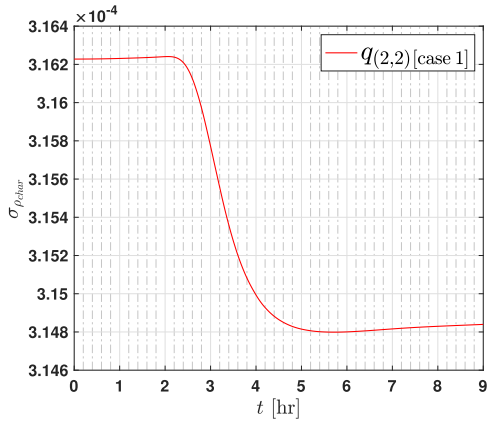

(a) Adaptation of process covariances $q_{(2,2)}$ of ρ_{char} for the case 1.

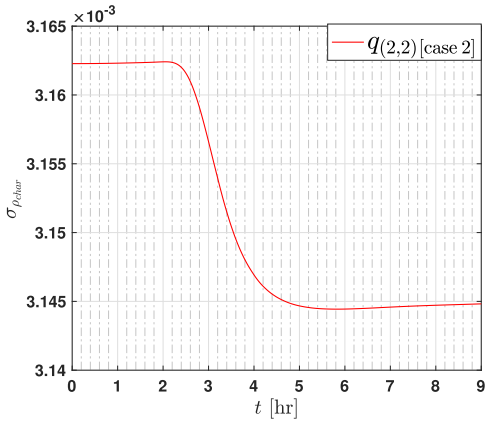

(b) Adaptation of process covariances $q_{(2,2)}$ of ρ_{char} for the case 2.

FIGURE 7. Adaptation of process covariances $q_{(2,2)}$ of ρ_{char}.

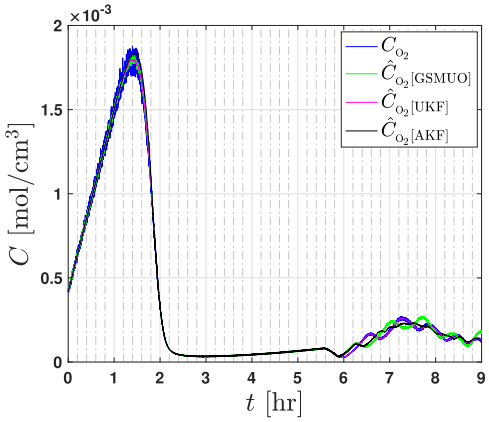

(a) Concentration of O_2

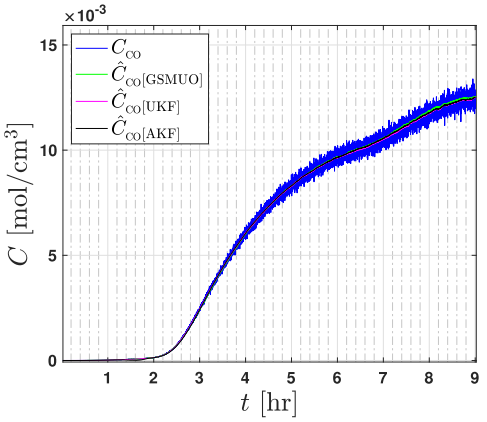

(b) Concentration of CO

FIGURE 8. Measured concentrations and their estimates for AKF, UKF and GSMUO.

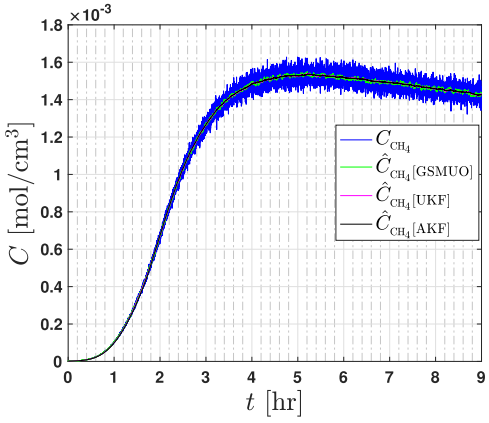

(a) Concentration of CH_4

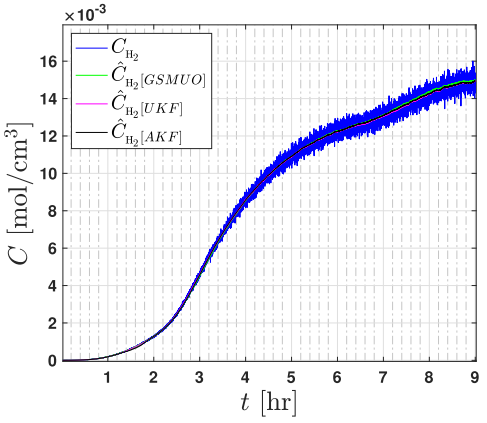

(b) Concentration of H_2

FIGURE 9. Measured concentrations and their estimates for AKF, UKF and GSMUO.

the initial values for $\boldsymbol{Q}_0$ and $\boldsymbol{R}_0$ for AKF and UKF are selected as given in Case 1. Furthermore, the noise cancellation due to adaptation of $\boldsymbol{Q}_k$ and $\boldsymbol{R}_k$ in AKF is better as compared to UKF and GSMUO. This can be seen in zoomed view of Fig. (10-b). The concentration of gases are shown in Figs. (8–11 and 13 b), in which O_2, N_2 and H_2O are inlet

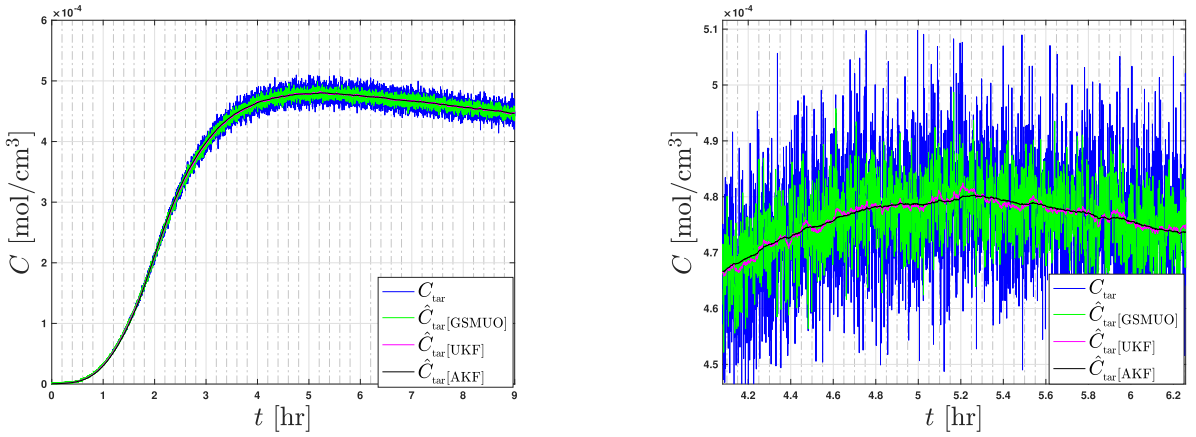

(a) Concentration of tar (b) Concentration of tar in zoomed view

FIGURE 10. Measured concentrations and their estimates for AKF, UKF and GSMUO.

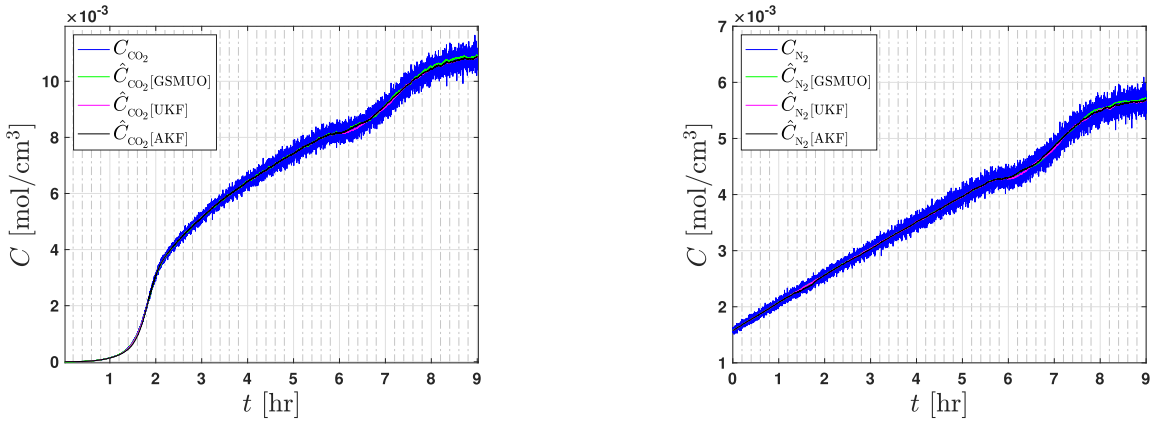

(a) Concentration of CO_2 (b) Concentration of N_2

FIGURE 11. Measured concentrations and their estimates for AKF, UKF and GSMUO.

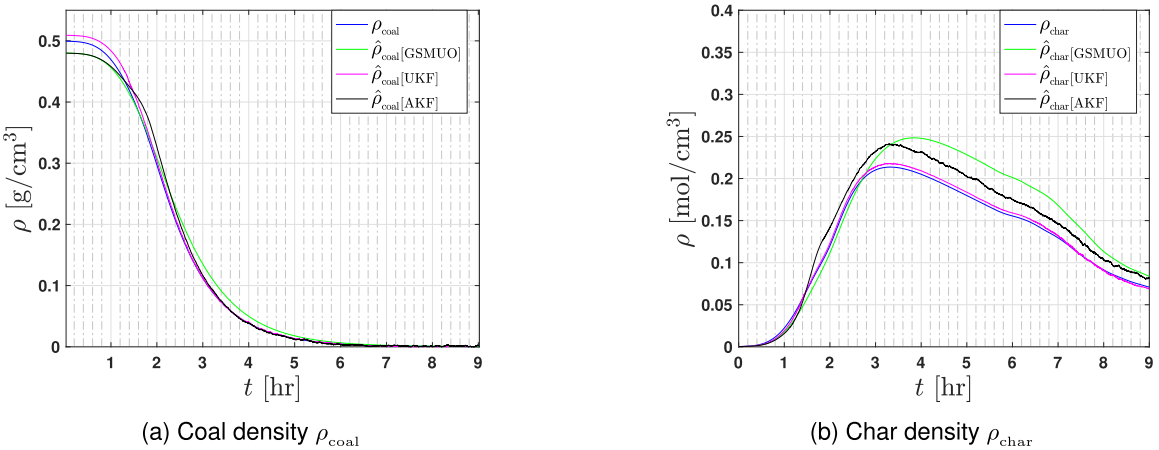

(a) Coal density ρ_{coal} (b) Char density ρ_{char}

FIGURE 12. Actual and estimated states of the UCG process for AKF, UKF and GSMUO.

gases which are manipulated by the controller to maintain the desired H_v and smooth consumption of char. The product gases CO, CO_2, H_2 and tar are formed in their respective chemical reactions as given in Table (1). It can be seen from Figs. (8–11 and 13 b) that AKF cancels out both process and measurement noises effectively.

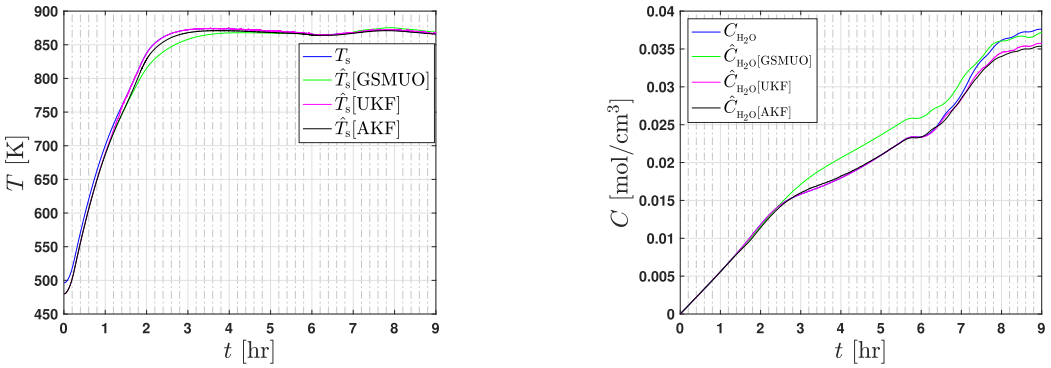

(a) Solid Temperature T_s (b) Concentration of H_2O

FIGURE 13. Actual and estimated states of the UCG process for AKF, UKF and GSMUO.

TABLE 7. Performance comparison in terms of $\tilde{e}_{\text{rms}}$ for AKF and UKF against different process and sensor noise covariances Q_0, R_0.

	Case-1		Case-2		Case-3	
Content	**AKF**	**UKF**	**AKF**	**UKF**	**AKF**	**UKF**
ρ_{coal}	0.010	0.005	0.0106	0.0107	0.0103	0.031
ρ_{char}	0.018	0.003	0.017	0.032	0.0180	0.045
T_s	6.89	5.19	6.908	11.57	6.847	67.41
H_2O	0.0009	0.0007	0.0009	0.001	0.0009	0.006

As discussed in section (IV) only product gases are available at the outlet of the well. Hence, the remaining four unknown states of the UCG model are reconstructed by using different estimators. It can be seen from Figs. (12–13), that both designed KFs are better than the GSMUO. As discussed earlier that these results are shown only for the Case-1 where response of AKF is close to UKF. However, for worst cases (Case 2, 3) when initial biased values of covariance matrices $\boldsymbol{Q}_0$ and $\boldsymbol{R}_0$ are high, the performance of UKF is deteriorated as depicted in terms of $\tilde{e}_{\text{rms}}$ in Table (7). Hence, the performance of AKF is more robust than UKF.

VI. CONCLUSION

In this work, a model-based constrained linear MPC is designed to track the desired heating value to its predefined set-points such that maximum efficiency of a UCG process can be achieved. The designed MPC also handles constraints on the control input which are imposed due to installed compressors' limitations. The MPC requires the states of the plant which are estimated through AKF, UKF and GSMUO. It is worth mentioning that both control and estimator design approaches (MPC and AKF) are linear and developed by using quasi-linear decomposition of the nominal model of the UCG process. For assessing the robustness of the control strategies, parametric variations, input disturbance, and process and measurement noises are included in the UCG plant model. A comprehensive comparison has been made between different control strategies, i.e., MPC-AKF, MPC-UKF and MPC-GSMUO. The simulation results and quantitative analysis demonstrate that MPC-AKF outperforms the other strategies in terms of e_{rms} and p_{avg}. Moreover, a quantitative analysis has been carried for AKF and UKF, which shows that the performance of AKF is more robust against the change in the initial values of measurement and process covariances.

Some future extensions of this work may include the estimation of disturbance and uncertain parameters, which is expected to improve the performance of the control scheme.

REFERENCES

[1] N. Abas, A. Kalair, and N. Khan, "Review of fossil fuels and future energy technologies," *Futures*, vol. 69, pp. 31–49, May 2015.
[2] N. V. Gnanapragasam, B. V. Reddy, and M. A. Rosen, "Hydrogen production from coal gasification for effective downstream CO_2 capture," *Int. J. Hydrogen Energy*, vol. 35, no. 10, pp. 4933–4943, May 2010.
[3] M. Liszka, T. Malik, M. Budnik, and A. Zięb ik, "Comparison of IGCC (integrated gasification combined cycle) and CFB (circulating fluidized bed) cogeneration plants equipped with CO_2 removal," *Energy*, vol. 58, pp. 86–96, Sep. 2013.
[4] K. R. Jillson, V. Chapalamadugu, and B. Erik Ydstie, "Inventory and flow control of the IGCC process with CO_2 recycles," *J. Process Control*, vol. 19, no. 9, pp. 1470–1485, Oct. 2009.
[5] M. Mansouri Majoumerd, H. Raas, S. De, and M. Assadi, "Estimation of performance variation of future generation IGCC with coal quality and gasification process—Simulation results of EU H2-IGCC project," *Appl. Energy*, vol. 113, pp. 452–462, Jan. 2014.
[6] N. S. Siefert and S. Litster, "Exergy and economic analyses of advanced IGCC–CCS and IGFC–CCS power plants," *Appl. Energy*, vol. 107, pp. 315–328, Jul. 2013.
[7] D. A. Bell, B. F. Towler, and M. Fan, "Underground coal gasification," in *Coal Gasification its Applications*. Boston, MA, USA: William Andrew, 2011, pp. 35–71.
[8] G. Perkins and V. Sahajwalla, "A mathematical model for the chemical reaction of a semi-infinite block of coal in underground coal gasification," *Energy Fuels*, vol. 19, no. 4, pp. 1679–1692, 2005.
[9] G. Perkins, "Underground coal gasification—Part I: Field demonstrations and process performance," *Prog. Energy Combustion Sci.*, vol. 67, pp. 158–187, Jul. 2018.
[10] G. Perkins, "Underground coal gasification—Part II: Fundamental phenomena and modeling," *Prog. Energy Combustion Sci.*, vol. 67, pp. 234–274, Jul. 2018.
[11] M. Green, "Recent developments and current position of underground coal gasification," *Proc. Inst. Mech. Eng., A, J. Power Energy*, vol. 232, no. 1, pp. 39–46, Feb. 2018.
[12] A. A. Uppal, A. I. Bhatti, E. Aamir, R. Samar, and S. A. Khan, "Control oriented modeling and optimization of one dimensional packed bed model of underground coal gasification," *J. Process Control*, vol. 24, no. 1, pp. 269–277, 2014.
[13] J. Kacur and M. Durdan, "The investigation of UCG control methods," in *Proc. 15th Int. Multidisciplinary Sci. Geoconf. (SGEM)*, Jun. 2015, pp. 375–382.
[14] K. Kostúr and J. Kačúr, "The monitoring and control of underground coal gasification in laboratory conditions," *Acta Montanistica Slovaca*, vol. 13, no. 1, pp. 111–117, 2008.
[15] K. Kostúr and J. Kačúr, "Development of control and monitoring system of UCG by promotic," in *Proc. 12th Int. Carpathian Control Conf. (ICCC)*, May 2011, pp. 215–219.
[16] J. Kačur, M. Durdán, M. Laciak, and P. Flegner, "A comparative study of data-driven modeling methods for soft-sensing in underground coal gasification," *Acta Polytechnica*, vol. 59, no. 4, pp. 322–351, Aug. 2019.

[17] K. Kostúr and J. Kačur, "Extremum seeking control of carbon monoxide concentration in underground coal gasification," *IFAC-PapersOnLine*, vol. 50, no. 1, pp. 13772–13777, Jul. 2017.
[18] Y. Xiao, J. Yin, Y. Hu, J. Wang, H. Yin, and H. Qi, "Monitoring and control in underground coal gasification: Current research status and future perspective," *Sustainability*, vol. 11, no. 1, p. 217, Jan. 2019.
[19] livermore, P. Flegner, M. Durdán, and M. Laciak, "Model predictive control of UCG: An experiment and simulation study," *Inf. Technol. Control*, vol. 48, no. 4, pp. 557–578, 2019.
[20] J. Kačur, M. Laciak, M. Durdán, and P. Flegner, "Model-free control of UCG based on continual optimization of operating variables: An experimental study," *Energies*, vol. 14, no. 14, p. 4323, Jul. 2021.
[21] H. Satyavada and S. Baldi, "Monitoring energy efficiency of condensing boilers via hybrid first-principle modelling and estimation," *Energy*, vol. 142, pp. 121–129, Jan. 2018.
[22] A. A. Uppal, A. I. Bhatti, E. Aamir, R. Samar, and S. A. Khan, "Optimization and control of one dimensional packed bed model of underground coal gasification," *J. Process Control*, vol. 35, pp. 11–20, Nov. 2015.
[23] A. A. Uppal, Y. M. Alsmadi, V. I. Utkin, A. I. Bhatti, and S. A. Khan, "Sliding mode control of underground coal gasification energy conversion process," *IEEE Trans. Control Syst. Technol.*, vol. 26, no. 2, pp. 587–598, Mar. 2018.
[24] M. Khattak, A. A. Uppal, Q. Khan, A. I. Bhatti, Y. M. Alsmadi, V. I. Utkin, and I. Chairez, "Neuro-adaptive sliding mode control for underground coal gasification energy conversion process," *Int. J. Control*, pp. 1–12, 2021. [Online]. Available: https://www.tandfonline.com/doi/full/10.1080/00207179.2021.1909745?scroll=top&needAccess=true, doi: 10.1080/00207179.2021.1909745.
[25] A. Arshad, A. I. Bhatti, R. Samar, Q. Ahmed, and E. Aamir, "Model development of UCG and calorific value maintenance via sliding mode control," in *Proc. Int. Conf. Emerg. Technol.*, Oct. 2012, pp. 1–6.
[26] A. A. Uppal, S. S. Butt, A. I. Bhatti, and H. Aschemann, "Integral sliding mode control and gain-scheduled modified utkin observer for an underground coal gasification energy conversion process," in *Proc. 23rd Int. Conf. Methods Models Autom. Robot. (MMAR)*, Aug. 2018, pp. 357–362.
[27] A. A. Uppal, S. S. Butt, Q. Khan, and H. Aschemann, "Robust tracking of the heating value in an underground coal gasification process using dynamic integral sliding mode control and a gain-scheduled modified Utkin observer," *J. Process Control*, vol. 73, pp. 113–122, Jan. 2019.
[28] A. M. Chaudhry, A. A. Uppal, Y. M. Alsmadi, A. I. Bhatti, and V. I. Utkin, "Robust multi-objective control design for underground coal gasification energy conversion process," *Int. J. Control*, vol. 93, no. 2, pp. 328–335, 2018.
[29] S. B. Javed, A. A. Uppal, R. Samar, and A. I. Bhatti, "Design and implementation of multi-variable H_∞ robust control for the underground coal gasification project thar," *Energy*, vol. 216, Feb. 2021, Art. no. 119000.
[30] S. B. Javed, V. I. Utkin, A. A. Uppal, R. Samar, and A. I. Bhatti, "Data-driven modeling and design of multivariable dynamic sliding mode control for the underground coal gasification project thar," *IEEE Trans. Control Syst. Technol.*, early access, Mar. 1, 2021.
[31] C. B. Thorsness and J. A. Britten, "Lawrence Livermore national laboratory underground coal gasification project," Lawrence Livermore Nat. Lab., Livermore, CA, USA, Tech. Rep. UCID-21853, ON: DE90005752, 1989.
[32] M. C. M. Teixeira and S. H. Zak, "Stabilizing controller design for uncertain nonlinear systems using fuzzy models," *IEEE Trans. Fuzzy Syst.*, vol. 7, no. 2, pp. 133–142, Apr. 1999.
[33] M. Morari and J. H. Lee, "Model predictive control: Past, present and future," *Comput. Chem. Eng.*, vol. 23, nos. 4–5, pp. 667–682, May 1999.
[34] S. J. Qin and T. A. Badgwell, "A survey of industrial model predictive control technology," *Control Eng. Pract.*, vol. 11, no. 7, pp. 733–764, 2003.
[35] Y. A. Sha'aban, F. Tahir, P. W. Masding, J. Mack, and B. Lennox, "Control improvement using MPC: A case study of pH control for brine dechlorination," *IEEE Access*, vol. 6, pp. 13418–13428, 2018.
[36] L. Wang, *Model Predictive Control System Design and Implementation Using MATLAB*. London, U.K.: Springer, 2009.
[37] S. K. Godunov, "A difference method for numerical calculation of discontinuous solutions of the equations of hydrodynamics," *Matematicheskii Sbornik*, vol. 89, no. 3, pp. 271–306, 1959.
[38] E. F. Camacho and C. B. Alba, *Model Predictive Control*. London, U.K.: Springer-Verlag, 2007.
[39] I. Hashlamon and K. Erbatur, "An improved real-time adaptive Kalman filter with recursive noise covariance updating rules," *TURKISH J. Electr. Eng. Comput. Sci.*, vol. 24, no. 2, pp. 524–540, 2016.
[40] D. Simon, *Optimal State Estimation: Kalman, H Infinity, and Nonlinear Approaches*. Hoboken, NJ, USA: Wiley, 2006.
[41] Y. Song, M. Park, M. Seo, and S. W. Kim, "Online state-of-charge estimation for lithium-ion batteries considering model inaccuracies under time-varying current conditions," *IEEE Access*, vol. 8, pp. 192419–192434, 2020.
[42] S. Akhlaghi, N. Zhou, and Z. Huang, "Adaptive adjustment of noise covariance in Kalman filter for dynamic state estimation," in *Proc. IEEE Power Energy Soc. Gen. Meeting*, Jul. 2017, pp. 1–5.
[43] A. H. Mohamed and K. P. Schwarz, "Adaptive Kalman filtering for INS/GPS," *J. Geodesy*, vol. 73, no. 4, pp. 193–203, 1999.

AFRAZ MEHMOOD CHAUDHRY received the B.E. degree in electronics engineering from Air University Islamabad, in 2006, and the M.S. degree in computer engineering from the University of Engineering and Technology Taxila, Pakistan, in 2012. He is currently pursuing the Ph.D. degree in model predictive control of thermal grids with Vrije Universiteit Brussel (VUB). He started his career as a Load and Dispatch Engineer with the National Power Control Center, Pakistan, and then joined the Center of Excellence in Engineering Sciences to conduct research on clean energy convertible systems. In the last six years, he has been actively involved in control-oriented modeling, states and parameter estimation, model predictive control, and optimization of smart and clean energy systems.

ALI ARSHAD UPPAL (Member, IEEE) received the B.E. and M.S. degrees in electrical and computer engineering from the University of Engineering and Technology Taxila, Taxila, Pakistan, in 2006 and 2012, respectively, and the Ph.D. degree in electrical engineering from COMSATS University Islamabad (CUI), Pakistan, in 2016. He is currently working as a Postdoctoral Researcher on the UPWIND Project at the Department of Electrical and Computer Engineering, University of Porto. He is also an Assistant Professor with the Department of Electrical and Computer Engineering, CUI. So far, he has authored/coauthored 24 journal/conference publications with an aggregate impact factor of 70. His research interests include nonlinear control, sliding mode control, process control, numerical optimal control, control of infinite dimensional systems, and control of energy conversion systems.

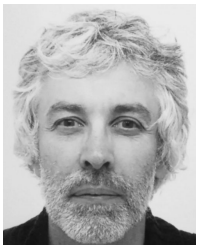

SVEND BRAM received the degree in electromechanical engineering from Vrije Universiteit Brussel (VUB), in 1990, and the Ph.D. degree in electro-mechanical engineering, on the topic of evaporative regeneration in gas turbine cycles, from VUB, in 2002. From 2002 to 2008, he worked with the Department of Mechanical Engineering (MECH), VUB, where he setup a T100 CHP microturbine test facility to perform experiments for flexible power production through steam and water injection. From 2008 to 2014, he was a Lecturer with the Department of Industrial Sciences and Technology (IWT), Erasmus University College Brussels (EhB), where he setup a laboratory for real-time measurements of particulate emissions from biomass combustion. Since October 2014, he has been a Professor with the Department of Engineering Technology (INDI), VUB. He is a member of European Turbine Network (ETN) and the Belgian Section of the Combustion Institute. He is teaching courses on thermodynamics, energy conversion systems, turbomachinery, HVAC, renewable energy technology, and jet engines. He is the Vice-Chairman of the Educational Council of the Faculty of Engineering and the Vice-Chairman of the Curriculum Board of industrial engineering.